

Engineering the electronic structure of TiO_2 by transition metal doping: A First Principles DFT Study

Vikash Mishra¹, Shashi Pandey², Swaroop Ganguly², Alok Shukla^{3*}

¹*Department of Physics, Manipal Institute of Technology, Manipal Academy of Higher Education, Manipal, 576104, Karnataka, India*

²*Department of Electrical Engineering Indian Institute of Technology Bombay, Powai, Mumbai 400076, India*

³*Department of Physics, Indian Institute of Technology Bombay, Powai, Mumbai 400076, India*

Abstract

By means of first-principles density-functional theory (DFT) calculations, we perform a comparative analysis of the electronic and magnetic properties of transition metal doped TiO_2 . The electronic band gaps of $\text{Ti}_x\text{M}_{1-x}\text{O}_2$, where M represents 3d-transition metals such as Sc, V, Cr, Mn, Fe, Co, Ni, Cu, and Zn, have been determined using the PBE functional within the generalized-gradient approximation (GGA) scheme, and hybrid HSE06 functional. In the context of pure TiO_2 , the partial density of states (PDOS) reveals that the electronic band gap emerges between the O-2p and Ti-3d orbitals. It is suggested that the Ti-3d (t_{2g}) states play a more prominent role in bonding compared to the Ti-3d (e_g) states. We performed DFT calculations to investigate the impact of doping with other 3d transition metal atoms leading to the emergence of impurity states within the band gap. The hybridization between the oxygen 2p orbitals and the titanium 3d orbitals in TiO_2 is altered by the introduction of doping with 3d transition metals because of the change in the oxidation state of titanium, shifting from solely 4+ to a combination of 4+ and 3+ states. The calculation of spin-polarized density demonstrates the emergence of ferromagnetic properties, particularly in titanium dioxide doped with chromium (Cr), manganese (Mn), and iron (Fe) with large magnetic moments. Our work demonstrates the significant impact of doping transition metals on TiO_2 , allowing for the precise manipulation of electrical and magnetic properties, and thus holds great potential for the development of spin-based memory devices with possible neuromorphic applications.

Email: shukla@phy.iitb.ac.in

Keywords: TiO_2 , Transition Metals, DFT, Magnetism, Density of states, Magnetic moment

Introduction

Wide band-gap transition-metal oxides, have attracted extensive research interest due to their structural flexibility, chemical stability, and diverse range of applications in photocatalysis, sensors, and transparent electronics [1-7]. In particular, TiO_2 , due to its tunable electronic and magnetic properties, is increasingly investigated for its potential to develop exciting properties such as localized defect states, modulation of carrier concentration, and even magnetic ordering through doping with 3d-transition-metal atoms [8-11]. In doped TiO_2 , these effects have led to observations of room-temperature ferromagnetism, resistive switching behavior, and enhanced photocatalytic activity, making it a versatile platform for both fundamental studies and device-oriented research. Despite these advances, the microscopic mechanisms driving these emergent behaviors remain poorly understood, underscoring the need for systematic experimental and theoretical investigations. For instance, recent studies have demonstrated the significance of titanium dioxide (TiO_2), or its doping with 3d-transition metal atoms, in elucidating the electronic characteristics in the vicinity of the Fermi level [12,13,14]. The investigation of changes in the magnetic characteristics of TiO_2 when doped with transition metals is important. Numerous theoretical studies have demonstrated that the introduction of transition metals into TiO_2 results in the emergence of a magnetic moment in the vicinity of the dopant atom, as well as in its nearest neighboring atoms. Similarly, Extensive experimental studies on 3d-transition-metal doped TiO_2 (i.e. Co^{2+} and Fe^{3+} dopants) have reported emergent phenomena including room-temperature ferromagnetism, enhanced conductivity, and improved photocatalytic activity. In Co-doped anatase TiO_2 , strong magneto-optical effects and saturation magnetizations up to $\sim 1 \mu_B/\text{Co}$ have been observed [8,9]; however, detailed spectroscopic (i.e. XPS, ESR) and microscopic studies reveal that ferromagnetism often arises from the intrinsic point defects (e.g., Ti^{3+} or Ti vacancies) or from Co clustering rather than uniform substitutional doping. Oxygen-deficient processing conditions (e.g., vacuum annealing) tend to enhance ferromagnetic ordering by promoting bound magnetic polarons or vacancy-mediated exchange, whereas oxidizing conditions suppress it due to the formation of nonmagnetic phases. Similarly, Fe-doped and Fe–Cu co-doped TiO_2 powders exhibit robust room-temperature ferromagnetism arising from overlapping magnetic polarons and vacancy defects [10, 11]. Consequently, the investigation of the characterization of these materials in the solid-state phase has become a subject of interest for various research groups. However, thus far, the majority of research has

focused on experimental approaches, with limited attention given to first principle calculations [15-18]. Several previous studies have examined the electronic band structure and electronic density of states of pure metal oxides [8,14]. However, the investigation of comparative impurity effects in wide band gap semiconductors remains unexplored. The existence of three prevalent crystal forms, namely Anatase, Rutile, and Brookite, is widely acknowledged in the scientific community for the compound TiO_2 .

A study carried out in 2002; Park et al. [13] achieved successful growth of ferromagnetic Co-doped rutile TiO_2 films [19-21]. The Curie temperature (T_C) was calculated to be above 400 K for Co with a doping level of 12%. The present study investigates the electrical and magnetic characteristics of transition metal-doped TiO_2 , specifically $\text{Ti}_{1-x}\text{M}_x\text{O}_2$, where M represents a range of 3d-transition metals including Sc, V, Cr, Mn, Fe, Co, Ni, Cu, and Zn. In photocatalytic applications, anatase is frequently chosen over rutile due to its higher band gap, which results in a longer charge-carrier lifetime and increased photocatalytic activity [18]. Keeping this in view we have focused our current investigation on the anatase phase of TiO_2 [22]. The presence of magnetism in Fe-doped rutile TiO_2 film has been revealed by experimental investigation [20]. Similarly, the introduction of Cu-doping in rutile TiO_2 also results in a significant magnetic moment, which can be attributed to the existence of oxygen vacancies [21,23]. However, as far as current knowledge is concerned, there has been no comparative investigation conducted on the electronic structure and magnetism of 3d-transition metal doped anatase TiO_2 . The phenomenon of magnetism in transition-metal doped TiO_2 can be comprehended through spin polarization resulting from alterations caused by the dopant atom. This leads to the promotion of an electron from the t_{2g} orbitals to the e_g orbitals, which can induce varying modifications in the surrounding environment. The lower transition metals exhibit significant spin-orbit coupling, leading to the occurrence of Pseudo Jahn-Teller distortions [24-26] in octahedral structures. These distortions result in changes in spin polarization, which have been found in the $\text{O}_1\text{-Ti}\text{-O}_2$ bonds as well as the $\text{O}_1\text{-M}\text{-O}_2$ bonds in the $\text{Ti}_{1-x}\text{M}_x\text{O}_2$ compound. The enhancement of magnetic moments inside the system is a consequence of the alteration in spin polarization. Conversely, it is commonly acknowledged that the dependence of TM d-d transitions [27,28] on the hybridization of the doping orbitals with the host element is also recognized. The d-d transition occurring between the t_{2g} and e_g orbitals in the $\text{O}_1\text{-Ti}\text{-O}_2\text{-M}\text{-O}_1\text{-Ti}\text{-O}_2$ structure of metal-doped TiO_2 results in modifications in spin polarity, which varies depending on the dopant atom (M) incorporated into

the TiO_2 lattice. The band gap of transition metal-doped TiO_2 is not directly associated with the band gap between the Ti t_{2g} (d_{xy} , d_{xz} , d_{yz}) and e_g (dz^2 , dx^2-y^2) bands. Instead, it is determined by the energy separation between the overlapping of O-2p and the Ti-3d bands of TiO_2 . Consequently, this characteristic is also influenced by the presence of doping atoms.

In this present work we have performed a comparative study on the magnetic and electronic properties of 3d-transition metal doped anatase TiO_2 using a density-functional theory (DFT) based first principles approach. We have performed calculations using various approximations, however, results obtained from the HSE06 calculations were found to be very close to the experimental values. For the 3d-transition metal doped structures $\text{Ti}_x\text{M}_{1-x}\text{O}_2$ ($\text{M}=\text{Sc}$, V Cr , Mn , Fe , Co , Ni , Cu , Zn)[14], the HSE06 calculations were performed the using $2\times 2\times 1$ super cells. The DFT band structure calculations on the doped structures reveal the presence of impurity bands in the midgap region caused by the hybridization between O-2p, Ti-3d, and M-3d orbitals causing a change in oxidation state of Ti from 4+ to mixed states (i.e., 4+ and 3+). The spin-polarized projected DOS calculations confirm ferromagnetic behavior for most of the compounds, while the maximum magnetic moments can be seen especially in Cr, Mn and Fe doped TiO_2 .

Methods and Computational Details:

Density-functional theory was employed to perform spin-polarized calculations for the total energy as well as the band structure and projected density of states (PDOS). These calculations utilized projected-augmented wave (PAW) potentials and were carried out using the Quantum Espresso (QE) simulation software [29–34]. The results of the HSE06 calculations were found to be very close to the experimental values, despite the fact that we had also done preliminary calculations using various approximations, including LDA and the generalized gradient approximation (GGA) utilizing the PBE functional to verify the bandgap values. The calculations were performed on the super cell consisting of two-unit cells arranged in a stacked manner along the a-axes. For the anatase phase of TiO_2 , the super cell consists of 48 atoms in all, with 16 Ti atom and 32 O atoms ($\text{Ti}_{16}\text{O}_{32}$), in which one titanium (Ti) atom is substituted with a 3d-transition metal atom (denoted as M) selected among the atoms: Scandium (Sc), Vanadium (V), Chromium (Cr), Manganese (Mn), Iron (Fe), Cobalt (Co), Nickel (Ni), Copper (Cu), and Zinc (Zn). The crystal structures of the anatase phase of TiO_2 and the 3d-doped TiO_2

are depicted in figure 1, where the Ti atoms are represented by blue spheres, the O atoms by green spheres, and the transition metal dopant atoms by red spheres. The convergence of the total energy with respect to the size of the k-mesh is shown in figure 2(a) based on which we used $7 \times 7 \times 1$ k-mesh and for density of states calculations we have $13 \times 13 \times 1$ k-mesh. The super cells of the doped structures have the chemical formula $Ti_{15}M_1O_{32}$ ($M = Sc, V, Cr, Mn, Fe, Co, Ni, Cu, Zn$), amounting to a doping concentration of 6.25%. Both the pure and doped TiO_2 structures are fully relaxed until the forces/atom approach $0.04 \text{ eV}/\text{\AA}$ and an energy convergence of $5 \times 10^{-5} \text{ eV}$ is reached in order to guarantee correct results. A 400 eV kinetic energy threshold [35,36] was used in our computations.

Results and Discussion:

Prior to the calculations of electronic and magnetic properties of the systems under consideration, we optimized the geometry of each structure. From Figure 2 (b) it is clearly seen that due to doping the optimized lattice are different in each case. Experimentally, the band gap of titanium dioxide has been estimated around 3.22 eV from various reports with the indirect band gap nature[4,37]. To match with experimental bandgap we have tried various approximations such as LDA, GGA using the PBE functional, and the hybrid functional HSE06 [30]. LDA is the most basic DFT functional, based on the idea that the electron density at a particular location is the only factor influencing the exchange-correlation energy there [17]. In general, it underestimates band gaps and can result in inaccurate lattice parameters and other characteristics, despite its computational efficiency. PBE is a generalized gradient approximation (GGA) functional that incorporates the electron density gradient into the exchange-correlation energy computation, thereby improving upon LDA [12]. PBE tends to underestimate band gaps but generally outperforms LDA for structural features like cohesive energies and lattice constants. It's a widely used functional due to its balance between accuracy and computational cost. The hybrid functional HSE06 introduces non-local exchange interactions by combining Hartree-Fock exchange with a screened Coulomb potential. HSE06 is a widely used option for investigating electronic properties because of this non-local exchange, which is essential for accurately estimating band gaps [31]. Compared to LDA or PBE, HSE06 calculations require more computing power but frequently yield noticeably more precise band gaps [1,18,30,38,39]. The band gap of TiO_2 computed using various approximations has been tabulated in table-1, and it is found that using the HSE06 functional, it is nearly $\sim 3.2 \text{ eV}$ which is extremely close to the

experimental value 3.22 eV[4,37]. Here no extra electron correlation term has been added, i.e., no U has been used in our calculations.

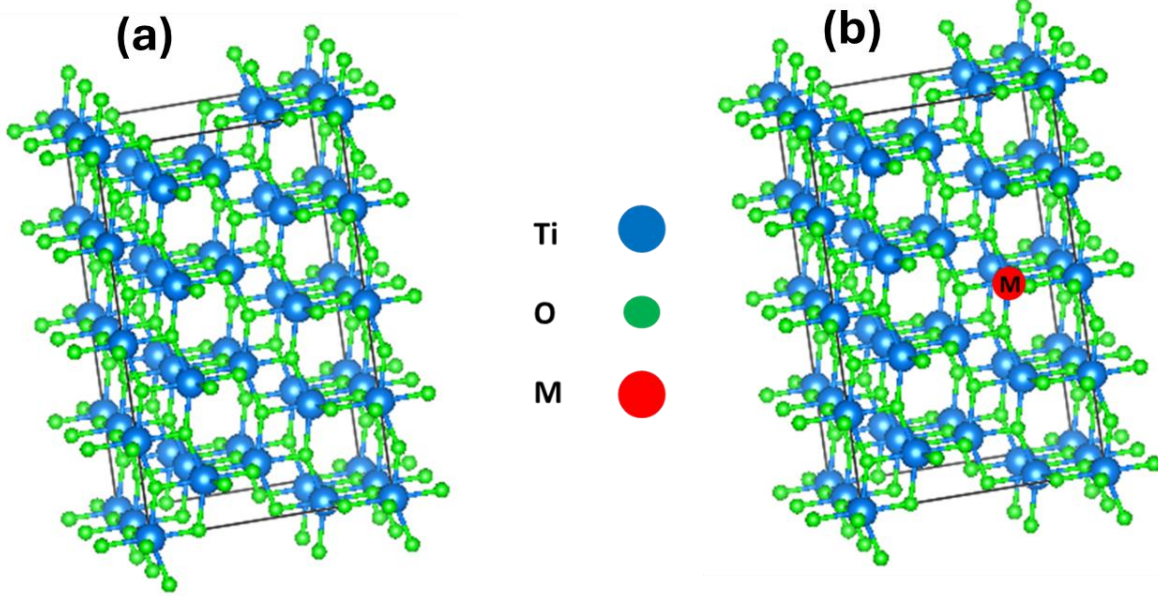


Figure 1: Anatase structure of (a) Pure TiO_2 and (b) Doped TiO_2 with 2x2x1 supercell. Blue green and red color indicates Ti, O and M ($M = Sc, V, Cr, Mn, Fe, Co, Ni, Zn$) atoms, respectively.

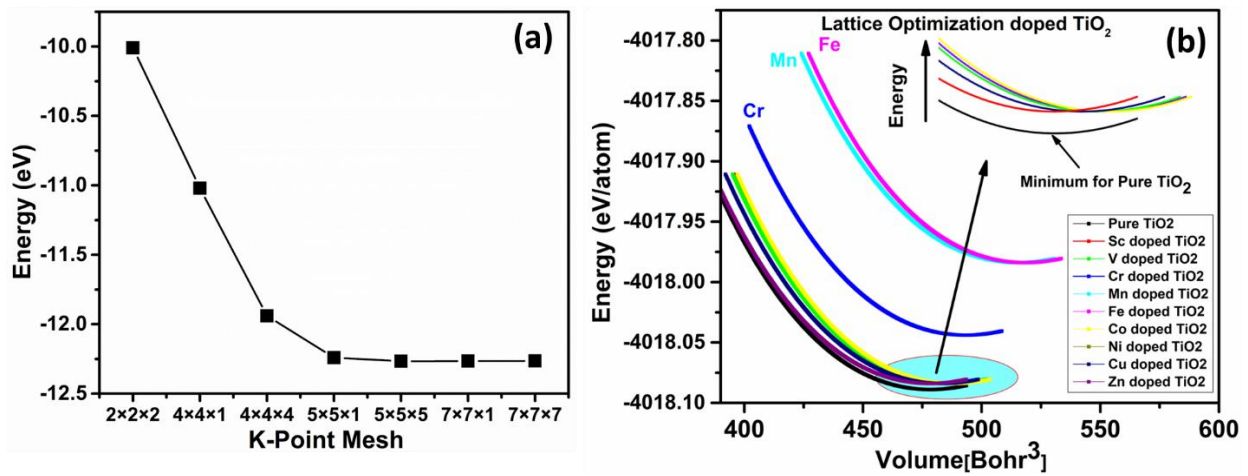


Figure 2: (a) K-point Mesh convergence and (b) Structural optimization of pure and doped TiO_2 .

Table-1: Estimation of Band gap of pure TiO_2 with various approximations.

Approximations	Pure TiO_2 Band Gap (in eV)
LDA	2.51
GGA-PBE	2.72
HSE06	3.20 (\sim close to experimental value 3.22 eV[4,37])

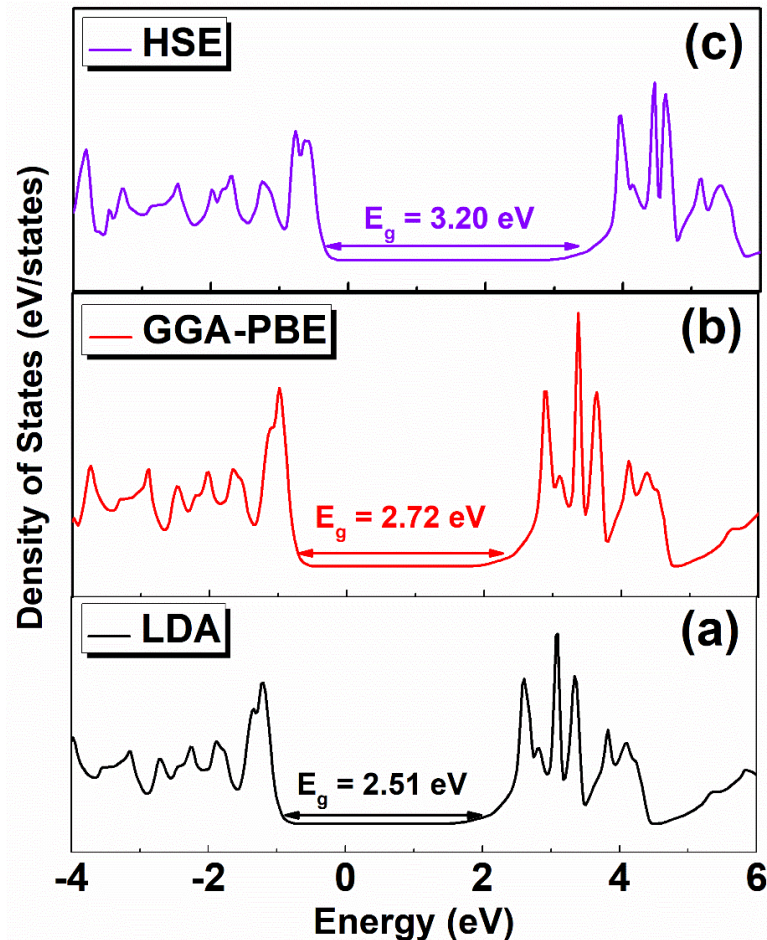


Figure-3: Total density of states (TDOS) for pure TiO_2 using (a) LDA (b) GGA (using PBE functional) and (c) HSE06 approximations.

In Figure 3 we have plotted calculated TDOS, obtained using various exchange-correlation functionals, for the pure TiO_2 . In the case of pure TiO_2 , the energy states near the Fermi level (E_F) are primarily composed of the hybridized O-2p and Ti-3d orbitals (see Fig. 4(a)). Previously , it

was reported that in the case of pure TiO_2 , a more detailed examination of the Partial Density of States (PDOS) around the Fermi energy (E_f) reveals that the Ti-3d (t_{2g}) states exhibit a greater dominance and play a more significant role in the bonding compared to the Ti-3d (e_g) states, as determined using the GGA-based calculations[4, 38,39-42]. In the context of O-2p orbitals, it can be observed that the contributions of p_x , p_y , and p_z orbitals near the Fermi energy (E_f) are of comparable magnitudes. The PDOS of pure TiO_2 , as depicted in Fig. 4(a), has a distinct band gap of 3.20 eV between the VBM and CBM. This value for the band gap (E_g) aligns with experimental findings. Based on Fig. 4(a), it is evident that the emergence of a band gap in TiO_2 can be attributed to the hybridization of the O-2p (valence band maximum) orbital with the Ti-3d (conduction band minimum) orbital [1,4,43].

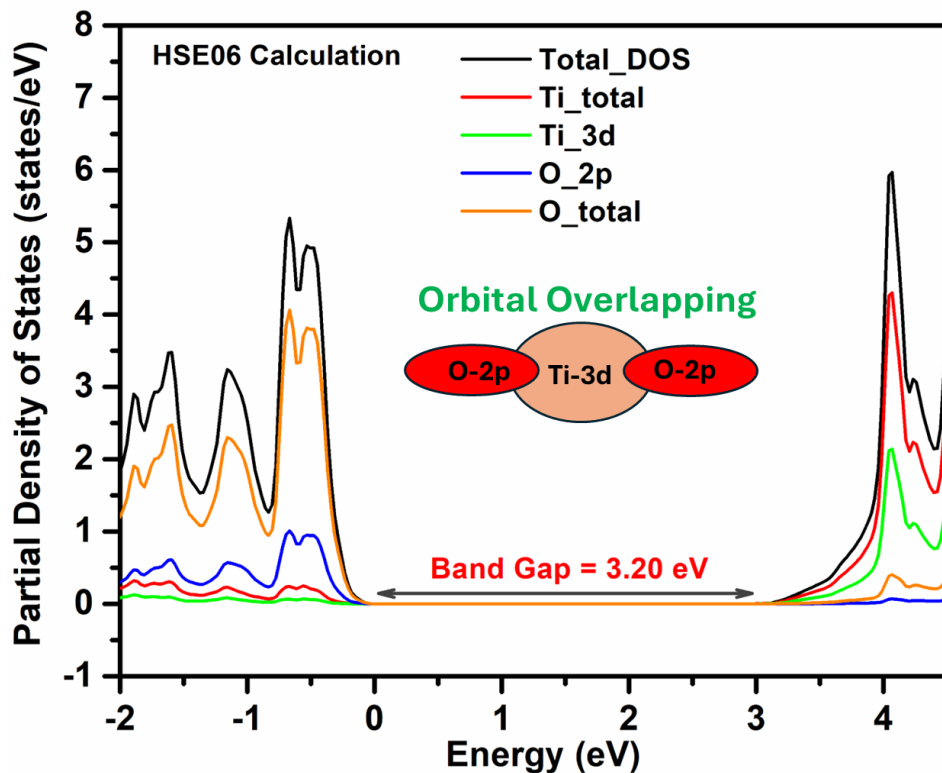


Figure-4(a): Partial density of states (PDOS) of pure anatase TiO_2 shows an electronic band gap of 3.20 eV, with the Ti-3d orbital exhibiting the maximum contribution near the conduction band minimum, while the O-2p orbitals dominate near the valance band maxima. The states near the Fermi energy display hybridization between O-2p and Ti-3d orbitals.

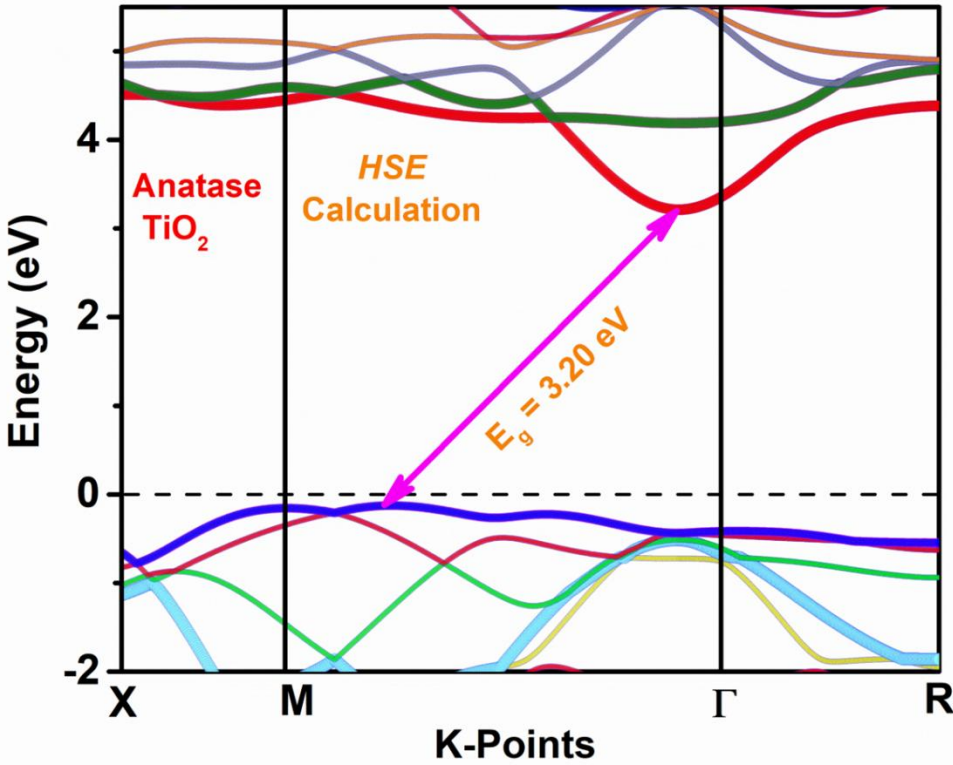


Figure-4 (b): Band structure of the pure anatase TiO_2 computed using the HSE06 functional.

Clearly, the band gap is indirect in nature.

To further confirm the orbital contribution and the nature of the band gap, band structure calculations for the pure TiO_2 have been depicted in Figure 4(b). From Fig. 4(b), It is clearly shown that anatase TiO_2 has an indirect nature of band gap of 3.20 eV between Γ and M points. To assess the structural stability of the doped systems, it is important to calculate their formation energies, for which we used the formula [37,38]

$$E_{form} = E_{Doping} - E_{Pure} + \sum_i n_i \mu_i, \quad (1)$$

where, E_{form} represents the formation energy of the given structure, E_{Doping} represents the total energy of the doped structure, E_{pure} represent the total energy of the pure structure, while n_i and μ_i denote the total number of the i -th atom, and its chemical potential. By including the contributions of the translational, rotational, and vibrational degrees of freedom of a material, it is possible to compute its free energy. However, given the high computational costs of such calculations, we have performed all our calculations at 0K temperature (i.e., avoided the room

temperature calculations ~ 298 K) [44-46]. Hence, we have used the reported values of chemical potential [45, 46] needed in equation-1, and with the help of calculated total energy of the pure and doped structures, we have estimated their formation energies.

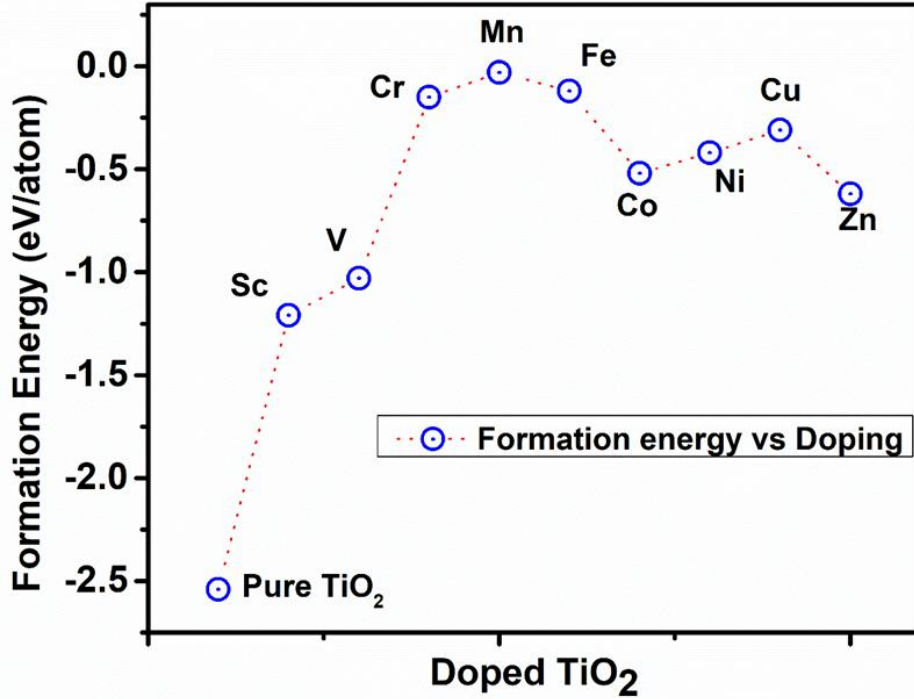


Figure 5: The calculated formation energies of pure and 3d-doped TiO_2 .

The calculated formation energies are presented in Fig. 5 from which it is obvious for all the cases the formation energies are negative indicating that it is possible to synthesize these structures in a laboratory [17,43]. The spin-polarized density of states (SPDOS) of the 3d-transition metal doped structures of the anatase TiO_2 , i.e., $\text{Ti}_x\text{M}_{1-x}\text{O}_2$, have been computed using the HSE06 functional [4], and presented in Figure 6 (a-i). It is observed that several extra states appear in between valance band and conduction bands for different dopants (i.e. impurity states). Consequently, the number and the nature of the midgap impurity states will be different for each dopant. Furthermore, the occupied and the virtual states available for the eletctronic transitions will also be different as compared to the pure titanium dioxide (TiO_2), leading to distinct electronic properties for the 3d transition metal doped TiO_2 [47,48].

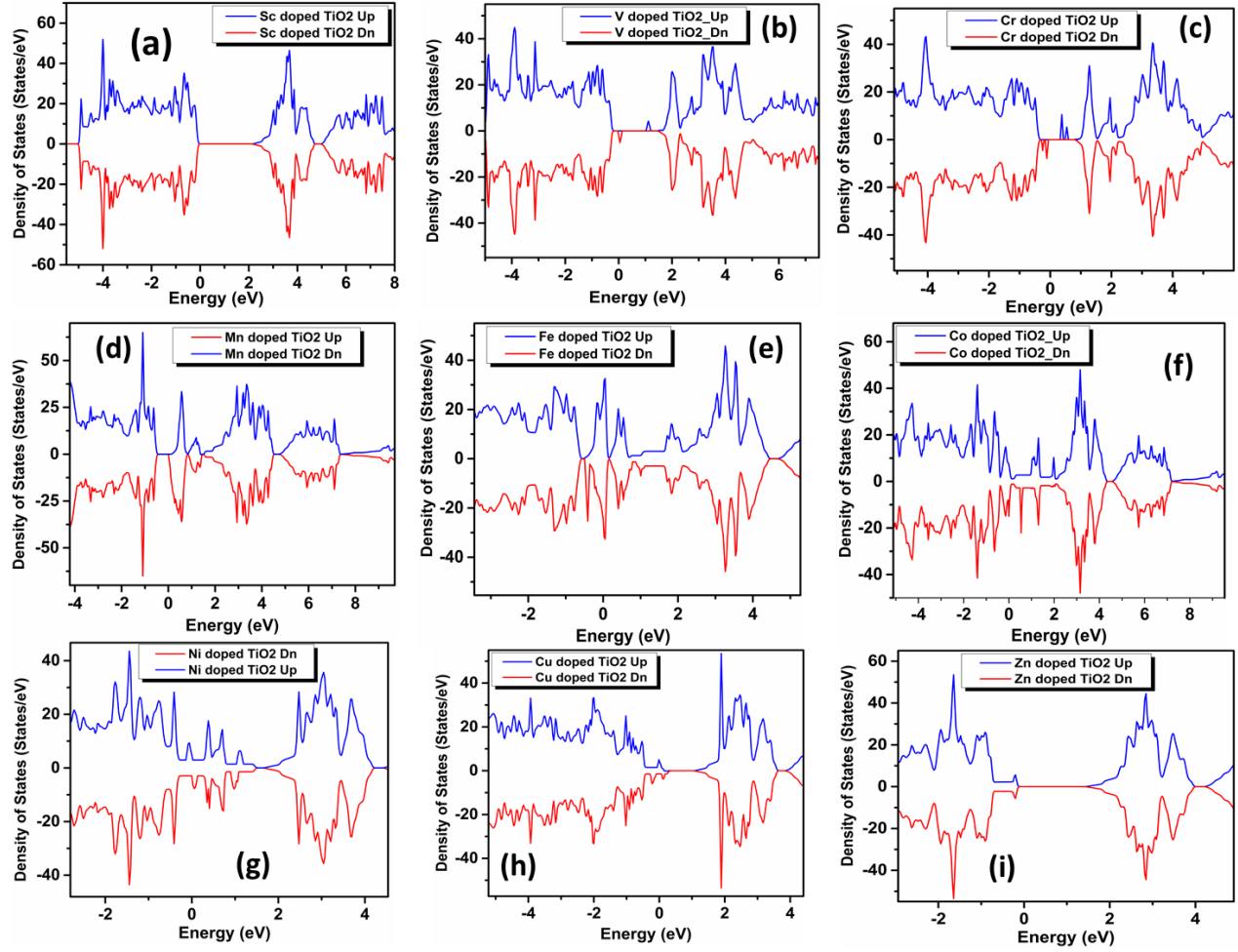


Figure-6: Spin polarized density of states (SPDOS) for 3d-transition metal doped TiO_2 with $2x2x1$ supercells: (a) $Ti_{15}Sc_1O_{32}$ (b) $Ti_{15}V_1O_{32}$ (c) $Ti_{15}Cr_1O_{32}$ (d) $Ti_{15}Mn_1O_{32}$ (e) $Ti_{15}Fe_1O_{32}$ (f) $Ti_{15}Co_1O_{32}$ (g) $Ti_{15}Ni_1O_{32}$ (h) $Ti_{15}Cu_1O_{32}$ (i) $Ti_{15}Zn_1O_{32}$.

In the SPDOS, the shifting of the electronic states from CBM and VBM to the mid-gap region with the increase in the atomic number of the the dopant atoms clearly implies the existence of variable oxidation states of 3d-transition metal atoms ($Sc=+3$, $V= +2,+3,+4,+5$, $Cr= +2,+3,+4,+6$, $Mn= +2,+3,+4,+6,+7$ $Fe=+2,+3+6$, $Co=+2,+3$, $Ni=+2,+3$, $Cu= -1,+2,+3$, $Zn=+2$) causing the hybridization between O-2p and Ti-3d to change. Different dopants (i.e. transition metal atoms) have different number of unpaired electrons in their 3d orbital and hence we obtain different up- and down- SPDOS, leading to the onset of ferromagnetic behavior[9,19,49]. Band structure calculations for three representative cases (a) V (b) Mn, and (c) Ni doped TiO_2 have been performed using the HSE06 functional to further confirm the presence of impurity states in

between CBM and VBM, as shown in figure 7 (a)-(c). From the band structure it is obvious that the total number of mid-gap states increase from one to three as the dopant changes from V to Mn, pointing to their dependence on the number of dopant 3d electrons.

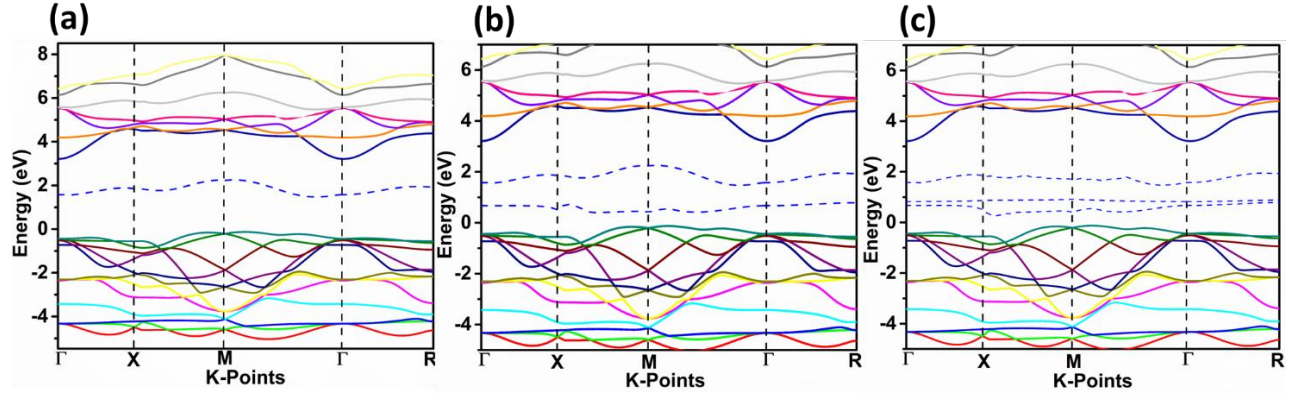


Figure 7: Band structure of (a) V (b) Mn and (c) Ni doped TiO_2 computed using the HSE06 functional. Solid lines represent electronic states corresponding to bulk bands, while the dashed lines represent defect states due to the corresponding dopants.

We have also calculated magnetic moments for all cases of doping, and the results are presented in Table 2, and we find that the maximum magnetic moments of $2.45\mu_B$, $3.57\mu_B$, $4.60\mu_B$, respectively, are induced at the doping sites for the dopants Cr, Mn and Fe. This clearly is due to a large number of unpaired electrons in 3d orbital of these atoms, consistent with the Hund's rule. Due to orbital hybridization, the neighboring oxygen atom also acquires very small magnetic moments.

Table-2 Calculated magnetic moments of metal doped TiO_2 at: (a) dopant sites, and (b) O atoms nearest to the dopant atoms

System	(a) Magnetic moment at the dopant site (in μ_B)	(b) Magnetic moment at the O atom nearest to the dopant atom (in μ_B)
$Ti_{15}Sc_1O_{32}$	0	$0(O_1), 0(O_2)$
$Ti_{15}V_1O_{32}$	0.9	$0.01(O_1), 0.01(O_2)$
$Ti_{15}Cr_1O_{32}$	2.45	$0.02(O_1), 0.03(O_2)$
$Ti_{15}Mn_1O_{32}$	3.57	$0.02(O_1), 0.03(O_2)$

$Ti_{15}Fe_1O_{32}$	4.60	0.04(O ₁),0.04(O ₂)
$Ti_{15}Co_1O_{32}$	1.42	0.05(O ₁),0.04(O ₂)
$Ti_{15}Ni_1O_{32}$	0.10	0.02(O ₁),0.03(O ₂)
$Ti_{15}Cu_1O_{32}$	1.02	0.02(O ₁),0.03(O ₂)
$Ti_{15}Zn_1O_{32}$	0.34	0.01(O ₁),0.01(O ₂)

Conclusions

In conclusion, to see the effect of doping of transition metal ions in anatase TiO₂, a comparative study has been performed using a density functional approach. The electronic structure of the 3d-transition metal doped Ti_xM_{1-x}O₂ (M=Sc, V Cr, Mn, Fe, Co, Ni, Cu, Zn) has been examined, and values of band gaps estimated using both the PBE functional within the GGA scheme, and the hybrid HSE06 functional. The presence of midgap states is a consequence of doping, and for the case of doping with Cr, Mn, and Fe, our calculations predict large magnetic moments at the dopant sites. Therefore, we believe that Cr-, Mn-, and Fe-doped anatase TiO₂ can serve as effective dilute magnetic semiconductors, with tremendous possibilities of spintronic applications.

Acknowledgments

VM sincerely thank to the Department of Physics, MIT Manipal for providing funding from the institute. Indian Institute of Technology Bombay, India is acknowledged by one of the authors (SP) for providing the Institute Postdoctoral fellowship.

Compliance with ethical standards:

Conflict of interest: The authors declare that they do not have any conflict of interest.

Data availability statement –

The raw/processed data required to reproduce these findings cannot be shared at this time as the data also forms part of an ongoing study.

References

- [1] V. Mishra, M.K. Warshi, A. Sati, A. Kumar, V. Mishra, A. Sagdeo, R. Kumar, P.R. Sagdeo, Diffuse reflectance spectroscopy: An effective tool to probe the defect states in wide band gap semiconducting materials, *Materials Science in Semiconductor Processing*. 86 (2018) 151–156. <https://doi.org/10.1016/j.mssp.2018.06.025>.
- [2] J. Robertson, Band offsets of wide-band-gap oxides and implications for future electronic devices, *Journal of Vacuum Science & Technology B*. 18 (2000) 1785–1791. <https://doi.org/10.1116/1.591472>.
- [3] G.Z. Xing, Y.H. Lu, Y.F. Tian, J.B. Yi, C.C. Lim, Y.F. Li, G.P. Li, D.D. Wang, B. Yao, J. Ding, Y.P. Feng, T. Wu, Defect-induced magnetism in undoped wide band gap oxides: Zinc vacancies in ZnO as an example, *AIP Advances*. 1 (2011) 022152. <https://doi.org/10.1063/1.3609964>.
- [4] V. Mishra, M.K. Warshi, A. Sati, A. Kumar, V. Mishra, R. Kumar, P.R. Sagdeo, Investigation of temperature-dependent optical properties of TiO₂ using diffuse reflectance spectroscopy, *SN Appl. Sci.* 1 (2019) 241. <https://doi.org/10.1007/s42452-019-0253-6>.
- [5] A. Sati, A. Kumar, V. Mishra, K. Warshi, A. Sagdeo, S. Anwar, R. Kumar, P.R. Sagdeo, Direct correlation between the band gap and dielectric loss in Hf doped BaTiO₃, *J Mater Sci: Mater Electron.* (2019). <https://doi.org/10.1007/s10854-019-01128-z>.
- [6] A. Sati, V. Mishra, A. Kumar, M.K. Warshi, A. Sagdeo, R. Kumar, P.R. Sagdeo, Effect of structural disorder on the electronic and phononic properties of Hf doped BaTiO₃, *J Mater Sci: Mater Electron.* 30 (2019) 9498–9506. <https://doi.org/10.1007/s10854-019-01281-5>.
- [7] V. Mishra, A. Kumar, A. Sagdeo, P.R. Sagdeo, Comparative structural and optical studies on pellet and powder samples of BaTiO₃ near phase transition temperature, *Ceramics International*. 46 (2020) 3250–3256. <https://doi.org/10.1016/j.ceramint.2019.10.030>.
- [8] K. A. Griffin, A. B. Pakhomov, C. M. Wang, S. M. Heald, & Kannan M. Krishnan, Intrinsic Ferromagnetism in Insulating Cobalt Doped Anatase TiO₂, *Phys. Rev. Lett.* 94, 157204 (2005). <https://doi.org/10.1103/PhysRevLett.94.157204>
- [9] J.-Y. Kim, J.-H. Park, B.-G. Park, H.-J. Noh, S.-J. Oh, J. S. Yang, D.-H. Kim, S. D. Bu, T.-W. Noh, H.-J. Lin, H.-H. Hsieh, and C. T. Chen, Ferromagnetism Induced by Clustered Co

in Co-Doped Anatase TiO_2 Thin Films, Phys. Rev. Lett. 90, 017401 (2003). <https://doi.org/10.1103/PhysRevLett.90.017401>.

[10] S. Yang, D. Jiang, & Zeng, Q. Room temperature ferromagnetism of Fe-doped and (Fe, Cu)-codoped TiO_2 powders prepared by mechanical alloying, J Mater Sci: Mater Electron 27, 6570–6577 (2016). <https://doi.org/10.1007/s10854-016-4602-6>

[11] LT. Tseng, X. Luo, T.T. Tan, S. Li & J. Yi, Doping concentration dependence of microstructure and magnetic behaviours in Co-doped TiO_2 nanorods, Nanoscale Res Lett 9, 673 (2014). <https://doi.org/10.1186/1556-276X-9-673>.

[12] A. Rubio-Ponce, A. Conde-Gallardo, D. Olguín, First-principles study of anatase and rutile TiO_2 doped with Eu ions: A comparison of GGA and LDA+U calculations, Phys. Rev. B. 78 (2008) 035107. <https://doi.org/10.1103/PhysRevB.78.035107>.

[13] W.K. Park, R.J. Ortega-Hertogs, J.S. Moodera, A. Punnoose, M.S. Seehra, Semiconducting and ferromagnetic behavior of sputtered Co-doped TiO_2 thin films above room temperature, Journal of Applied Physics. 91 (2002) 8093–8095. <https://doi.org/10.1063/1.1452650>.

[14] T. Umebayashi, T. Yamaki, H. Itoh, K. Asai, Analysis of electronic structures of 3d transition metal-doped TiO_2 based on band calculations, Journal of Physics and Chemistry of Solids. 63 (2002) 1909–1920. [https://doi.org/10.1016/S0022-3697\(02\)00177-4](https://doi.org/10.1016/S0022-3697(02)00177-4).

[15] R. Long, N.J. English, Y. Dai, First-Principles Study of S Doping at the Rutile TiO_2 (110) Surface, J. Phys. Chem. C. 113 (2009) 17464–17470. <https://doi.org/10.1021/jp904775g>.

[16] Y. Wang, R. Zhang, J. Li, L. Li, S. Lin, First-principles study on transition metal-doped anatase TiO_2 , Nanoscale Res Lett. 9 (2014) 46. <https://doi.org/10.1186/1556-276X-9-46>.

[17] S. Pandey, A. Shukla, A. Tripathi, Effect of pressure on electrical and optical properties of metal doped TiO_2 , Optical Materials. 133 (2022) 112875. <https://doi.org/10.1016/j.optmat.2022.112875>.

[18] L.-H. Ye, N. Luo, L.-M. Peng, M. Weinert, A.J. Freeman, Dielectric constant of NiO and LDA+U, Phys. Rev. B. 87 (2013) 075115. <https://doi.org/10.1103/PhysRevB.87.075115>.

[19] W.T. Geng, K.S. Kim, Structural, electronic, and magnetic properties of a ferromagnetic semiconductor: Co-doped TiO_2 rutile, Phys. Rev. B. 68 (2003) 125203. <https://doi.org/10.1103/PhysRevB.68.125203>.

[20] R. Suryanarayanan, V.M. Naik, P. Kharel, P. Talagala, R. Naik, Room temperature ferromagnetism in spin-coated anatase- and rutile- $Ti_{0.95}Fe_{0.05}O_2$ films, *J. Phys.: Condens. Matter.* 17 (2005) 755–762. <https://doi.org/10.1088/0953-8984/17/4/017>.

[21] S. Duhalde, M.F. Vignolo, F. Golmar, C. Chilitotte, C.E.R. Torres, L.A. Errico, A.F. Cabrera, M. Rentería, F.H. Sánchez, M. Weissmann, Appearance of room-temperature ferromagnetism in Cu-doped $TiO_{2-\delta}$ films, *Phys. Rev. B.* 72 (2005) 161313. <https://doi.org/10.1103/PhysRevB.72.161313>.

[22] T. Luttrell, S. Halpegamage, J. Tao, A. Kramer, E. Sutter & M. Batzill, Why is anatase a better photocatalyst than rutile? - Model studies on epitaxial TiO_2 films. *Sci Rep* 4, 4043 (2014). <https://doi.org/10.1038/srep04043>.

[23] L.A. Errico, M. Rentería, M. Weissmann, Theoretical study of magnetism in transition-metal-doped TiO_2 and $TiO_{2-\delta}$, *Phys. Rev. B.* 72 (2005) 184425. <https://doi.org/10.1103/PhysRevB.72.184425>.

[24] F.G. Anderson, Pseudo-Jahn-Teller effect for distortions involving oxygen and nitrogen impurities in silicon, *Phys. Rev. B.* 39 (1989) 5392–5396. <https://doi.org/10.1103/PhysRevB.39.5392>.

[25] I.B. Bersuker, N.B. Balabanov, D. Pekker, J.E. Boggs, Pseudo Jahn–Teller origin of instability of molecular high-symmetry configurations: Novel numerical method and results, *The Journal of Chemical Physics.* 117 (2002) 10478–10486. <https://doi.org/10.1063/1.1520132>.

[26] V. Polinger, P. Garcia-Fernandez, I.B. Bersuker, Pseudo Jahn–Teller origin of ferroelectric instability in $BaTiO_3$ type perovskites: The Green’s function approach and beyond, *Physica B: Condensed Matter.* 457 (2015) 296–309. <https://doi.org/10.1016/j.physb.2014.09.048>.

[27] S. Singh, N. Rama, M.S. Ramachandra Rao, Influence of d-d transition bands on electrical resistivity in Ni doped polycrystalline ZnO , *Appl. Phys. Lett.* 88 (2006) 222111. <https://doi.org/10.1063/1.2208563>.

[28] K. Saito, Y. Eishiro, Y. Nakao, H. Sato, S. Sakaki, Oscillator Strength of Symmetry-Forbidden d-d Absorption of Octahedral Transition Metal Complex: Theoretical Evaluation, *Inorg. Chem.* 51 (2012) 2785–2792. <https://doi.org/10.1021/ic2017402>.

[29] A. Kumar, V. Mishra, M.K. Warshi, A. Sati, A. Sagdeo, R. Kumar, P.R. Sagdeo, Possible evidence of delocalized excitons in Cr-doped $PrFeO_3$: An experimental and theoretical

realization, *Journal of Physics and Chemistry of Solids.* 130 (2019) 230–235. <https://doi.org/10.1016/j.jpcs.2019.03.012>.

[30] V. Mishra, A. Sagdeo, V. Kumar, M.K. Warshi, H.M. Rai, S.K. Saxena, D.R. Roy, V. Mishra, R. Kumar, P.R. Sagdeo, Electronic and optical properties of BaTiO₃ across tetragonal to cubic phase transition: An experimental and theoretical investigation, *Journal of Applied Physics.* 122 (2017) 065105. <https://doi.org/10.1063/1.4997939>.

[31] P.E. Blöchl, Projector augmented-wave method, *Phys. Rev. B.* 50 (1994) 17953–17979. <https://doi.org/10.1103/PhysRevB.50.17953>.

[32] G. Kresse, J. Furthmüller, Efficient iterative schemes for ab initio total-energy calculations using a plane-wave basis set, *Phys. Rev. B.* 54 (1996) 11169–11186. <https://doi.org/10.1103/PhysRevB.54.11169>.

[33] A. Sumanth, V. Mishra, P. Pandey, M.S.R. Rao, T. Dixit, Investigations into the Role of Native Defects on Photovoltaic and Spintronic Properties in Copper Oxide, *IEEE Transactions on Nanotechnology.* (2022) 1–6. <https://doi.org/10.1109/TNANO.2022.3204587>.

[34] P. Giannozzi, S. Baroni, N. Bonini, M. Calandra, R. Car, C. Cavazzoni, D. Ceresoli, G.L. Chiarotti, M. Cococcioni, I. Dabo, A.D. Corso, S. de Gironcoli, S. Fabris, G. Fratesi, R. Gebauer, U. Gerstmann, C. Gougaussis, A. Kokalj, M. Lazzeri, L. Martin-Samos, N. Marzari, F. Mauri, R. Mazzarello, S. Paolini, A. Pasquarello, L. Paulatto, C. Sbraccia, S. Scandolo, G. Sclauzero, A.P. Seitsonen, A. Smogunov, P. Umari, R.M. Wentzcovitch, QUANTUM ESPRESSO: a modular and open-source software project for quantum simulations of materials, *J. Phys.: Condens. Matter.* 21 (2009) 395502. <https://doi.org/10.1088/0953-8984/21/39/395502>.

[35] S. Pandey, A. Shukla, A. Tripathi, Elucidating the influence of native defects on electrical and optical properties in semiconducting oxides: An experimental and theoretical investigation, *Computational Materials Science.* (2021) 111037. <https://doi.org/10.1016/j.commatsci.2021.111037>.

[36] P. Singh, V. Mishra, S. Barman, M. Balal, S.R. Barman, A. Singh, S. Kumar, R. Ramachandran, P. Srivastava, S. Ghosh, Role of H-bond along with oxygen and zinc vacancies in the enhancement of ferromagnetic behavior of ZnO films: An experimental

and first principle-based study, *Journal of Alloys and Compounds*. 889 (2021) 161663. <https://doi.org/10.1016/j.jallcom.2021.161663>.

[37] V. Mishra, M.K. Warshi, R. Kumar, P.R. Sagdeo, Design and development of in-situ temperature dependent diffuse reflectance spectroscopy setup, *J. Inst.* 13 (2018) T11003. <https://doi.org/10.1088/1748-0221/13/11/T11003>.

[38] Z. Hu, H. Metiu, Choice of U for DFT+U Calculations for Titanium Oxides, *J. Phys. Chem. C*, 115, 13, (2011), 5841–5845, <https://doi.org/10.1021/jp111350u>.

[39] B. J. Morgan, G. W. Watson, Intrinsic n-type Defect Formation in TiO₂: A Comparison of Rutile and Anatase from GGA+U Calculations, *J. Phys. Chem. C*, 114, 5, (2010), 2321–2328, <https://doi.org/10.1021/jp9088047>.

[40] G.U. von Oertzen, A.R. Gerson, The effects of O deficiency on the electronic structure of rutile TiO₂, *J. Phys. Chem. Solids*. 68 (2007) 324–330. doi:10.1016/j.jpcs.2006.09.023.

[41] K.A. Connelly, H. Idriss, The photoreaction of TiO₂ and Au/TiO₂ single crystal and powder surfaces with organic adsorbates. Emphasis on hydrogen production from renewables, *Green Chem.* 14 (2012) 260–280. doi:10.1039/C1GC15992E.

[42] M. Sotoudeh, S.J. Hashemifar, M. Abbasnejad, M.R. Mohammadizadeh, Ab-initio study of hydrogen doping and oxygen vacancy at anatase TiO₂ surface, *AIP Adv.* 4 (2014) 027129. doi:10.1063/1.4866982.

[43] V. Mishra, A. Sati, M.K. Warshi, A.B. Phatangare, S. Dhole, V.N. Bhoraskar, Harnath Ghosh, A. Sagdeo, V. Mishra, R. Kumar, P.R. Sagdeo, Effect of electron irradiation on the optical properties of SrTiO₃ : An experimental and theoretical investigations, *Mater. Res. Express.* 5 (2018) 036210. <https://doi.org/10.1088/2053-1591/aab6f5>.

[44] S. B. Zhang, & J.E. Northrup, (1991). Chemical potential dependence of defect formation energies in GaAs: Application to Ga self-diffusion. *Physical Review Letters*, 67(17), 2339. DOI: <https://doi.org/10.1103/PhysRevLett.67.2339>

[45] L-F Huang and J. M. Rondinelli*, Electrochemical phase diagrams for Ti oxides from density functional calculations, *Phys. Rev. B* 92, 245126,(2015) DOI: <https://doi.org/10.1103/PhysRevB.92.245126>.

[46] J. A. Quirk, V. K. Lazarov, K. P. McKennaJ., First-Principles Modeling of Oxygen-Deficient Anatase TiO₂ Nanoparticles *Phys. Chem. C*, 124, 43, 23637–23647 (2020), doi: <https://doi.org/10.1021/acs.jpcc.0c06052>.

- [47] R. Long, Y. Dai, G. Menga and B. Huanga, Energetic and electronic properties of X- (Si, Ge, Sn, Pb) doped TiO₂ from first-principles, Phys. Chem. Chem. Phys., 2009,11, 8165-8172, <https://doi.org/10.1039/B903298C>
- [48] S. Matsushima, K. Takehara, H. Yamane, K. Yamada, H. Nakamura, M. Arai, K. Kobayashi, First-principles energy band calculation for undoped and S-doped TiO₂ with anatase structure, Journal of Physics and Chemistry of Solids, 68, 2,(2007), 206-210,<https://doi.org/10.1016/j.jpcs.2006.10.011>.
- [49] K.M. Reddy, A. Punnoose, Mapping ferromagnetism in Ti_{1-x}Co_xO₂: Role of preparation temperature (200–900°C) and doping concentration (0.00015≤x≤0.1), Journal of Applied Physics. 101 (2007) 09H112. <https://doi.org/10.1063/1.2712020>.